



ELSEVIER

Tectonophysics 354 (2002) 195–210

TECTONOPHYSICS

www.elsevier.com/locate/tecto

Two-dimensional simulations of surface deformation caused by slab detachment

Susanne J.H. Buiter*, Rob Govers, M.J.R. Wortel

Vening Meinesz Research School of Geodynamics, Faculty of Earth Sciences, Utrecht University, Budapestlaan 4, 3584 CD Utrecht, The Netherlands

Received 13 December 2001; accepted 24 June 2002

Abstract

Detachment of the deeper part of subducted lithosphere causes changes in a subduction zone system which may be observed on the Earth's surface. Constraints on the expected magnitudes of these surface effects can aid in the interpretation of geological observations near convergent plate margins where detachment is expected. In this study, we quantify surface deformation caused by detachment of subducted lithosphere. We determine the range of displacement magnitudes which can be associated with slab detachment using numerical models. The lithospheric plates in our models have an effective elastic thickness, which provides an upper bound for rapid processes, like slab detachment, to the surface deformation of lithosphere with a more realistic rheology. The surface topography which develops during subduction is compared with the topography shortly after detachment is imposed. Subduction with a non-migrating trench system followed by detachment leads to a maximum surface uplift of 2–6 km, while this may be higher for the case of roll-back preceding detachment. In the latter situation, the back-arc basin may experience a phase of compression after detachment. Within the context of our elastic model, the surface uplift resulting from slab detachment is sensitive to the depth of detachment, a change in friction on the subduction fault during detachment and viscous stresses generated by sinking of the detached part of the slab. Overall, surface uplift of these magnitudes is not diagnostic of slab detachment since variations during ongoing subduction may result in similar vertical surface displacements.

© 2002 Elsevier Science B.V. All rights reserved.

Keywords: Slab detachment; Uplift; Subduction; Collision; Finite element method

1. Introduction

Observations from sites of present-day subduction and from former convergent plate margins indicate that the deeper part of subducted lithosphere may

mechanically decouple from the lithosphere at the surface. We refer to this process as slab detachment. Originally, detachment of subducted lithosphere at present-day regions of plate convergence was suggested on the basis of gaps in the hypocentral distribution associated with subducted slabs (e.g., [Isacks and Molnar, 1969](#)). Regional examples are Southern Italy ([Ritsema, 1972](#)), the New Hebrides ([Pascal et al., 1973](#)) and the Carpathians ([Fuchs et al., 1979](#)). More recently, gaps in subducted lithosphere were inferred

* Corresponding author. Present address: Institute of Geological Sciences, University of Bern, Baltzerstrasse 1, 3012 Bern, Switzerland. Tel.: +41-31-631-8760; fax: +41-31-631-4843.

E-mail address: susanne@geo.unibe.ch (S.J.H. Buiter).

from images of regional tomographic studies of, for example, the Carpathians (Oncescu et al., 1984), the Hellenic arc (Spakman et al., 1988) and Italy (Wortel and Spakman, 1992, 2000). An example of slab detachment at a former convergent plate margin may be found in the Asian region. In the Late Jurassic or Early Cretaceous, Siberia and Mongolia collided, closing the ocean in between. The subducted slab sank into the mantle and its remnants are presently imaged at depths of 1500 km and deeper (Van der Voo et al., 1999).

Detachment of subducted lithosphere is expected to cause changes in a subduction zone system which may be observed at the Earth's surface. Among the predicted surface effects are uplift (Westaway, 1993; Chatelain et al., 1992), a temporal change in stress regime (Hippolyte et al., 1994; Sorel et al., 1988; Meijer and Wortel, 1996), magmatism, metamorphism and rapid exhumation (Davies and Von Blanckenburg, 1995; Von Blanckenburg and Davies, 1995). To be able to recognise the expressions of slab detachment in geological observations, a knowledge of the magnitudes of the surface effects which may be expected is required. In this study, we, therefore, quantify surface effects of detachment of subducted lithosphere. Our focus lies on displacements of the Earth's surface. Through numerical modelling, we aim to identify the range of displacement magnitudes which can be associated with slab detachment. In a previous study (Buiter et al., 2001), we found that vertical surface displacements of a few kilometres may be induced during continuing convergence. Here we investigate whether surface displacements due to slab detachment can be distinguished from such displacements.

We consider two settings in which slab detachment may occur: (1) during closure of an ocean basin (Fig. 1a) and (2) during ongoing subduction (Fig. 1b). Fig. 1a shows a (hypothetical) example of the closing basin setting. More often than not the continental margins will be irregularly shaped. Collision at the promontories stops convergence between the continents. The remaining oceanic lithosphere can then only continue to subduct if roll-back and back-arc extensions are possible. An example of the closing of such an irregular ocean can be found in the Mediterranean region. Where the passive margins have been subducted, slab break-off may be initiated

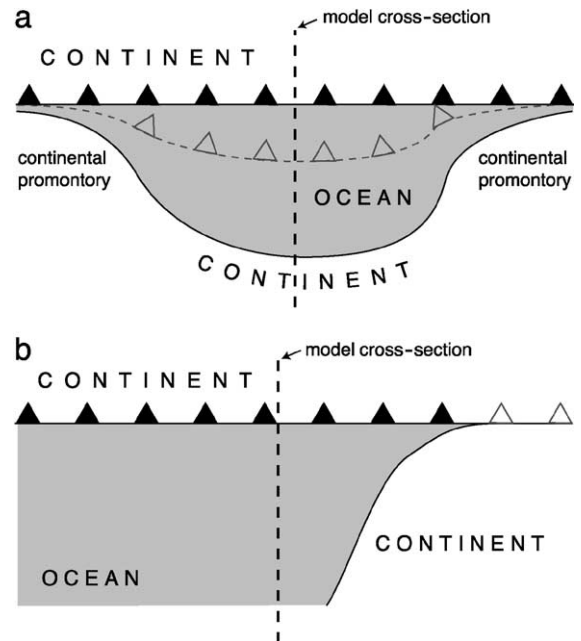


Fig. 1. (a) Sketch in map view of the closing of a hypothetical ocean with an irregular continental margin. Collision takes place first at the promontories. Subsequently, the remaining ocean basin can only be subducted through roll-back of the trench system (indicated by the dotted gray line). Collision at the promontories may trigger slab detachment which may subsequently propagate into the central part of the basin, i.e., our model section. (b) Alternatively, detachment of subducted lithosphere may occur in a 'normal' subduction setting with ongoing convergence between the two plates. Slab detachment may be initiated by subduction of a weak zone. In the map sketch shown here, it is implied that detachment is not initiated in the section of interest (indicated by the line labeled 'model cross-section'), but elsewhere for instance by the arrival of a continental margin at the trench. The detachment may then propagate laterally into the area under investigation.

(McKenzie, 1969; Davies and Von Blanckenburg, 1995; Wong et al., 1997). Such a tear in the slab may subsequently propagate horizontally into the central oceanic section.

The second setting which we consider is illustrated in Fig. 1b and represents ongoing convergence without roll-back. Subduction of a passive margin at the right initiates slab break-off, but the overall plate convergence continues. The tear propagates horizontally into the open ocean section. An example may be found in southeast Asia where the Eurasian and Australian plates collide in the Banda region, and where slab detachment may be occurring beneath Timor.

In both cases, detachment of subducted lithosphere could equally well result from the subduction of a zone of weakness, for example, subduction of a spreading ridge or a transform fault.

In a setting with subduction zone roll-back, retrograde motion of the subducted slab at depth is easiest when mantle material can flow around the slab (Dvorkin et al., 1993). This can, for example, be the case for a short slab or a slab which is narrow in the along-trench direction. In such a situation, the dip angle of the subducted slab may change during roll-back. In contrast, retrograde motion of long and/or wide slabs is probably more difficult in view of the large mantle pressures which have to be overcome. We expect that in that case, changes in the slab dip angle will be small.

To investigate the settings described above, we analyse the following models. In the closing basin setting, we consider models of slab roll-back involving a short and/or narrow slab (roll-back short: RS), and roll-back models with a long and wide slab (roll-back long: RL). The ongoing subduction setting (without roll-back) is analysed in models referred to as model S.

A few previous studies have quantified surface uplifts resulting from slab detachment. Mitrovica et al. (1989) show how post-Cretaceous uplift of Western North America, with a maximum vertical displacement of at least 3 km, might (partly) be explained by termination of subduction. They employ a viscous model in which the subducting slab is not continuous, but is built from separate lithospheric blocks. Schott and Schmeling (1998) use a viscous model to examine detachment of a delaminated mantle lithosphere. They obtain a topographic change of 1.6 km. Giunchi et al. (1996) and Carminati et al. (1999) use a viscoelastic model to investigate whether present-day surface velocities show a signature of slab detachment which occurred several millions of years ago. In these studies, detachment does not result in surface uplift. However, the authors do not include the process of detachment itself in their simulations, but start their calculations with an already detached slab.

Once slab detachment is complete, the detached part of the slab sinks into the mantle. This leads to dynamic mantle pressures which deflect the overlying surface downward. As the slab sinks further the pressures near the surface decrease and the depression

diminishes. Chatelain et al. (1992) focus on surface uplift caused by this sinking process only. We adopt their approach to take this effect on surface deflection into account.

2. Modelling method

We simulate the evolution of a convergent plate boundary in which subduction is followed by slab detachment. We focus on surface signals shortly after detachment occurred. In this way, we obtain surface displacements which are measured relative to the surface geometry of the preceding subduction phase. The phase of subduction is simulated in order to overcome initialisation signatures and obtain an internally consistent predetachment model.

2.1. Equations, rheology and geometry

We model subduction with a two-dimensional numerical method using the same approach as described in Buiter et al. (2001). Below, we describe the main features of the model. For more detailed aspects, we refer to the above-mentioned study. We solve the equations of mechanical equilibrium using the finite element code TECTON (Melosh and Raefsky, 1980, 1983; Melosh and Williams, 1989). The effect of large deformations is taken into account through the formulation of Wallace and Melosh (1994). The plane strain approximation is adopted.

On geological time scales, the response of the lithosphere to forcing is determined by a depth-dependent rheology which includes elastic, plastic and viscous behaviour. To mimic the bending of thick lithosphere with such a depth-dependent rheology, we use model plates with an effective elastic thickness (e.g., Watts and Talwani, 1974; Caldwell et al., 1976) (Fig. 2a). The magnitudes and distribution of stresses and strains in our elastic model will differ from those for a depth-dependent rheology. However, directly after loading, bending moments in the elastic model are identical to those for a realistic rheology and lithospheric thickness (Turcotte and Schubert, 1982). This means that surface deflections as predicted by our models are equal to those for a depth-dependent rheology, when considered shortly after changes in the subduction system occurred. In simulations of trench

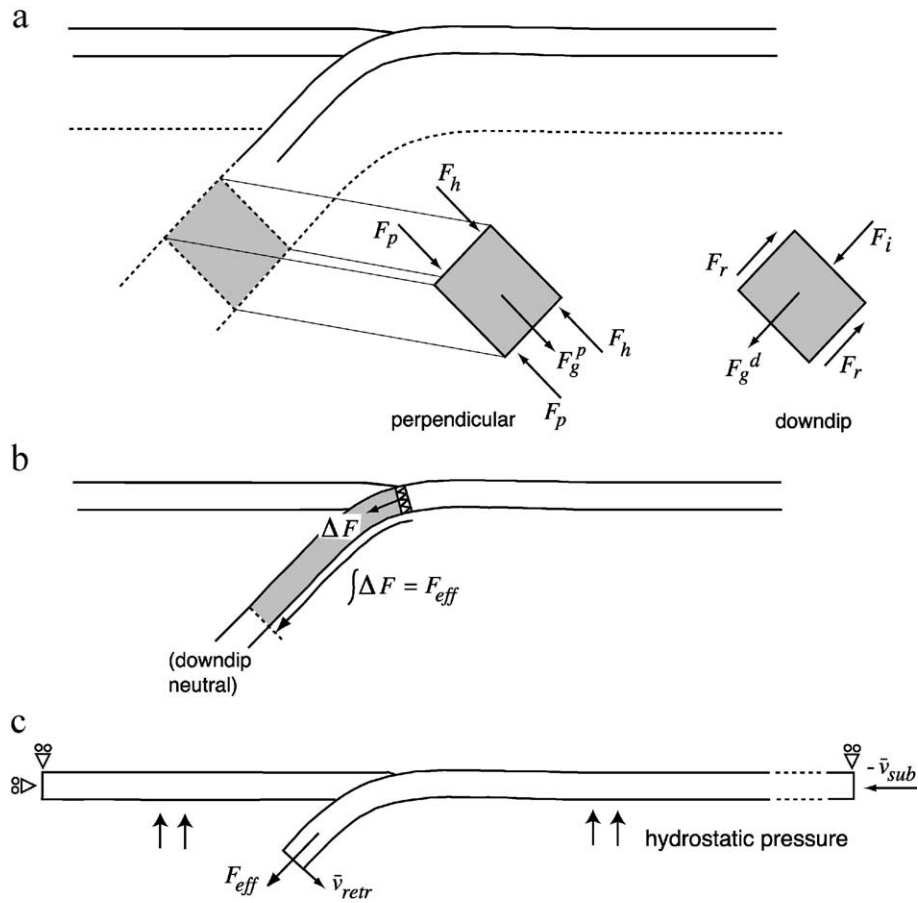


Fig. 2. (a) The behaviour of thick lithosphere (dotted line) is in the model approximated by using plates with an effective elastic thickness (drawn line). Forces acting on a fully subducted segment of the subducting plate are indicated: F_g slab pull, F_h hydrostatic restoring force, F_p force due to pressure differences, F_i ridge push, and F_r resistive force. (b) Subduction of a new slab segment at the trench (denoted with zigzags) generates a force increment ΔF . Integration of the force increments along the slab gives the total effective pull force F_{eff} . (c) Schematic illustration of the model and general boundary conditions. The subducting plate experiences an effective pull force (F_{eff}) oriented along dip of the slab. Subduction zone roll-back is simulated through a slab normal velocity (\bar{v}_{retr}) applied at the model slab end. The right hand side boundary of the subducting plate moves with a prescribed velocity while the left-hand side of the overriding plate is held fixed laterally. Both top corners at the left and right hand side are not allowed to move vertically. Figure is after Fig. 2 of Buiter et al. (2001).

roll-back, a local zone of weakness is introduced in the overriding plate to allow for back-arc extension. The weak zone is simulated by a zone of lower viscosity. This part of the model has a linear visco-elastic rheology.

Our models are started with the geometry of a short plate subducted beneath an overriding plate (Fig. 2). Because we are interested in subduction on longer time scales, this starting geometry requires that bending pre-stresses are incorporated in the bent part of the subducting plate. These prestresses allow for unbend-

ing at depth of subducted lithosphere in case of an elastic rheology. Bending stresses which are dynamically consistent with a subduction geometry are computed by flexing a horizontal plate by stresses at one plate end while the other end is held fixed. An overriding plate is subsequently added to the flexed plate to complete the initial geometry.

The asthenosphere is not explicitly included in the model domain. Instead, we have chosen to represent the effects of the asthenosphere on the lithosphere through pressure boundary conditions which act

directly on the model lithosphere (see Section 2.2.2). Subduction models which either incorporate the asthenosphere (e.g., Gurnis et al., 1996) or not (e.g., Hassani et al., 1997) all require the definition of boundary conditions on the model domain sides. In both cases, one has to be aware that the chosen boundary conditions can affect the processes under investigation. A larger model is not necessarily the better choice in all situations. For lithosphere models which do incorporate the asthenosphere, the choice of boundary conditions on the sides (e.g., rigid or in/out flow) or bottom (e.g., permeable or impermeable) of the computational domain affects slab behaviour (Davies, 1995; Christensen, 1996).

The contact between the subducting and overriding plate is a slippery fault (Melosh and Williams, 1989), which is allowed to deform, while differential displacements between the overriding and the subducting plate are locally always parallel to the fault geometry. The fault is free of friction.

2.2. Boundary conditions and forcing

2.2.1. Driving forces

Models for the subduction setting are driven on their right-hand side by a velocity at the surface (Fig. 2c). This boundary condition represents the net effect of both plate tectonic forces beyond the model domain and ridge push forces within the surface oceanic plate. The left-hand side is kept fixed. Models for the closing basin setting are held fixed at the surface on both sides.

The model slab experiences an effective pull force (F_{eff}) which is formed by the gravitational pull due to the density difference between slab and mantle, reduced by frictional resistive forces caused by its motion in the mantle. As new slab segments subduct, they generate a force increment ΔF (Fig. 2b). This force increment also consists of a driving contribution due to the density difference with the surrounding material and a counteractive contribution formed by resistive forces. We assume that, once the slab has straightened out, the along dip component of slab pull is locally balanced by viscous shear forces and internal lithospheric stresses. Force increments ΔF , therefore, only contribute to the effective pull force above a depth of approximately 150 km. Consequently, $F_{\text{eff}} = \int \Delta F dz$, where the integration is from the surface

to 150 km depth. For the case of non-migrating steady-state subduction (i.e., slab dip and velocity remain the same with time; model S0), the effective pull force amounts to $F_{\text{eff}}^0 = 2.4 \times 10^{13} \text{ N m}^{-1}$, directed along dip of the slab (Buiter et al., 2001). This value for the effective pull force and the associated force increments will be used as a reference, which is why they will be referred to as F_{eff}^0 and ΔF^0 . In the models, the force increment is applied in a shallow depth interval between 60 and 80 km. This forcing interval lies below the region of largest bending of the subducting plate and above the initial model slab end.

When towards the end of a subduction phase, passive margin material is being subducted, it is to be expected that the density difference between the subducting material and its surroundings reduces. This would then imply a reduction in the force increment ΔF .

2.2.2. Asthenosphere

We simulate the interaction of the asthenosphere with the lithospheric plates through boundary conditions. In our model formulation, this interaction includes a hydrostatic pressure, viscous drag and dynamic pressures.

At the viscosity of the asthenosphere (on the order of 10^{21} Pa s), the relaxation time of a viscoelastic (Maxwell) body is on the order of a few thousand years. Deviatoric stresses can, therefore, not be supported on longer time scales, which implies that mantle flow on geological time scales is driven by pressure gradients and that stresses are hydrostatic. In our numerical model, a hydrostatic pressure acts on all lithospheric boundaries which are in contact with the asthenosphere. We assume that the asthenosphere is incompressible.

Subduction leads to viscous and dynamic pressures which are superimposed on this hydrostatic pressure field. As a plate subducts into the mantle, it will experience a viscous resistance. This frictional drag exerted by the mantle on the sides and leading edge of the subducting lithosphere acts to reduce the effect of the along dip component of slab pull. In our model, we assume that once the slab has straightened out, the along dip component of slab pull is balanced by viscous mantle stresses and internal stresses in the subducted slab. When the slab has not yet straightened out, the along dip component of slab pull is not

completely balanced by other forces. This leads to the aforementioned effective force increments ΔF .

The orientation of the subducted slab in our models is determined by the balance between forces which act in a direction normal to the slab (Fig. 2a). In case of steady non-migrating subduction, we assume that the slab normal component of slab pull and dynamic stresses exerted on the slab by the mantle (e.g., corner flow) balance each other. Therefore, these forces do not contribute to slab dip changes. Retrograde motion of the slab can occur if these forces are not completely in balance. This can be due, for example, to a reduction in dynamic pressures caused by flow of mantle material around the slab in case of a short slab or a narrow (in the along strike direction) subduction zone. The effect of the out-of-balance pressures is simulated with a velocity boundary condition in the slab normal direction applied at the model slab end (v_{retr} in Fig. 2c). This boundary condition accounts for the effects of net slab-normal pressure differences both along the model slab and along the deeper part of the slab that is not physically included in the model.

2.3. Slab detachment

We impose geologically fast detachment of the subducted slab. The effects of, for example, stretching and thinning of the slab before detachment are, therefore, not incorporated in our simulations. We expect that in reality, a detachment process would take longer than the Maxwell relaxation time of the mantle (a few thousands of years for a viscosity of 10^{21} Pa s) and that, therefore, the elastic response of the mantle can be neglected. Detachment is imposed through the introduction of a slippery fault (Melosh and Williams, 1989) in the subducted lithosphere. The forces across this fault are relaxed completely. Detachment in the model is imposed at relatively shallow depths (80–130 km). These depths lie within the range of depths (around 50–300 km) determined from tomographic images (e.g., Spakman, 1990) and analyses of lithospheric strength (Davies and Von Blanckenburg, 1995; Wong et al., 1997; Van de Zedde and Wortel, 2001).

After detachment, a velocity boundary condition prescribes the detached part of the slab to sink vertically into the mantle. Sinking of the detached lithosphere will cause flow of the viscous mantle. The resulting pressure differences deflect overlying litho-

sphere downward. As the detached lithosphere sinks further, the pressures reduce and, as a consequence, the downward deflection diminishes also. As a result, the viscous flow will contribute to surface uplift on a longer time scale (order 100 ka) (Chatelain et al., 1992). To obtain a first-order estimate of the viscous effect of the sinking of the detached part, we use the equivalent of a sphere sinking in an infinite viscous medium below a free surface (Stokes flow) (Morgan, 1965; Chatelain et al., 1992). Our implementation is further discussed in Appendix A.

It should be realised that the results of our modelling experiments are constrained by the two-dimensional nature of the models. In the context of slab detachment, this means that our results describe detachment of subducted lithosphere which takes place at the same depth and time along the whole subduction zone. Also, the model simulates very fast detachment, while in reality detachment may be expected to require a certain timespan. In the quantification of surface displacements the effects of erosion, sedimentation or internal density differences are not included.

3. Modelling analysis

3.1. Reference models

3.1.1. Predetachment model

The phase of subduction should be sufficiently long in order that effects of initialisation have disappeared before the detachment phase is started. By monitoring the evolution of model geometry and stresses, we have verified that 80 km of convergence across the trench is sufficient for this purpose. We simulate two settings: subduction with a non-migrating trench system and roll-back in a land-locked basin setting (Fig. 1).

Table 1
Modelling parameters

Parameter	Value
Effective plate thickness	25 km
Young's modulus	5×10^{10} Pa
Poisson's ratio	0.25
Viscosity weak zone	10^{21} Pa s
Gravitational acceleration	9.80 m s^{-2}

Our reference model for the ongoing subduction setting (S0) is driven by the effective pull force ($F_{\text{eff}}=F_{\text{eff}}^0$) and a velocity v_{sub} of 4 cm/year to the left, which is imposed at the surface side boundary of the subducting plate (Fig. 2c). The overall convergence between both side boundaries of the model is 4 cm/year. Our results are not sensitive to the assumed velocity since, for the adopted elastic rheology, time only enters the equations through this velocity boundary condition. We verified that neither topography nor model stresses vary when evaluated at a given

amount of convergence, which was achieved using different convergence velocities. Table 1 gives the adopted values for parameters used in the modelling. Fig. 3I shows the results of non-migrating subduction after 2 Ma. The overriding plate margin has subsided nearly 4 km. The dip angle of the subducting slab approximately remains the same with time, although it is allowed to change dynamically. This model is the same as model 1 in Fig. 3 in Buiter et al. (2001).

In the reference models for a closing basin setting, retrograde motion of the subducting slab is achieved

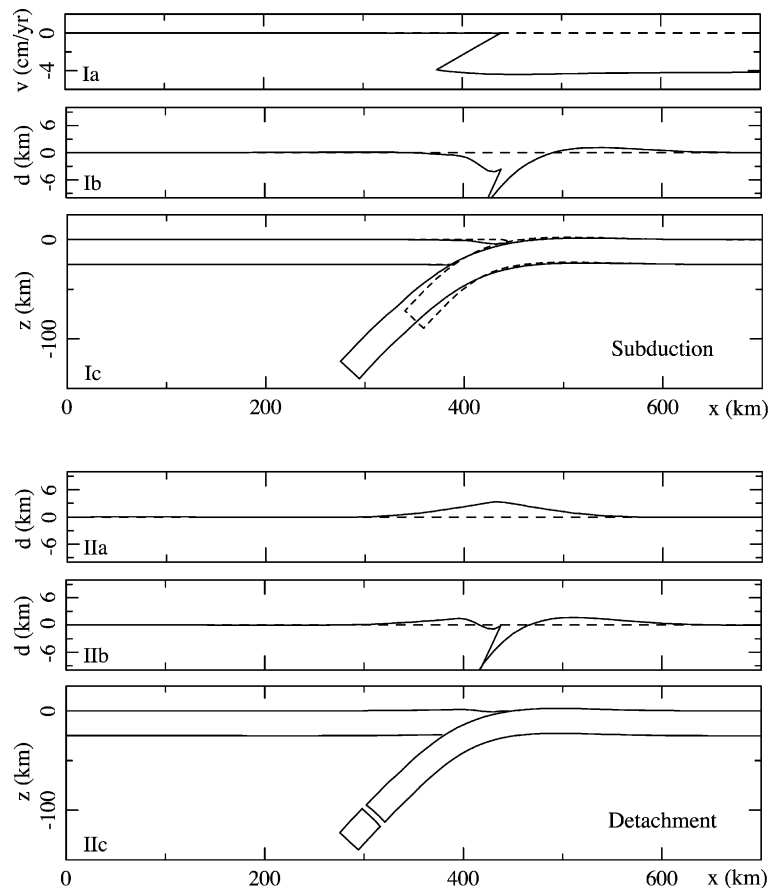


Fig. 3. Model S0. (I, top) Subduction of a negatively buoyant plate with a right hand side velocity boundary condition of 4 cm/year to the left. The subducting plate extends further to the right than shown here (initially to 1226 km). The subduction fault is free of friction. Results are shown after 2 Ma (80 km of convergence). (Ia) Horizontal surface velocity averaged over 0.1 Ma (dotted line denotes $v=0$ cm/year). (Ib) Vertical surface displacement relative to the surface of the initial model. (Ic) Outline of the model, dotted line is outline of the initial model. (II, below). Effect of detachment after 2 Ma of subduction. (IIa) Surface uplift due to detachment, displacement is relative to the surface of the model just before detachment. (IIb) Vertical surface displacement relative to the surface of the initial model. (IIc) Outline of the model. The small detached lithospheric slab is a numerical feature which is caused by the fact that the deeper part of the subducted slab is not included in the model domain. Its effects are represented by appropriate boundary conditions at the model slab end.

through a velocity v_{retr} of 2 cm/year applied at the model slab end. Both side boundaries of the surface plates are held fixed laterally. To allow for subduction zone roll-back, we introduce a 100 km wide weak zone (viscosity 10^{21} Pa s) in the overriding plate. In this area, extension localises and a back-arc basin forms. The slab retreat velocity for both models for a closing basin setting was selected so that the velocity of trench retreat falls within the range of values for present-day subduction zones (up to around 5 cm/year) (Garfunkel et al., 1986; DeMets et al., 1994).

In the first reference model for a closing basin setting, we assume that the subducted slab is relatively short (RS0). The dip angle of the slab is free to

change, since resulting changes in dynamic mantle pressures can be accommodated by flow of mantle material around the slab end. In 3.5 Ma of subduction zone roll-back, the dip angle of the slab increases by 16° (Fig. 4I). During this time, the trench retreats horizontally with 80 km at an average rate of 2.3 cm/year. The maximum subsidence of the overriding plate margin is around 4.0 km.

In the second reference model for a closing basin setting, we model a long and wide slab (RL0). Changes in dip angle of the deeper part of the slab are unlikely in view of the large slab normal pressures which have to be overcome. Therefore, the dip angle of the model slab end is constrained. After 2.5 Ma, the maximum subsidence of the overriding plate margin is

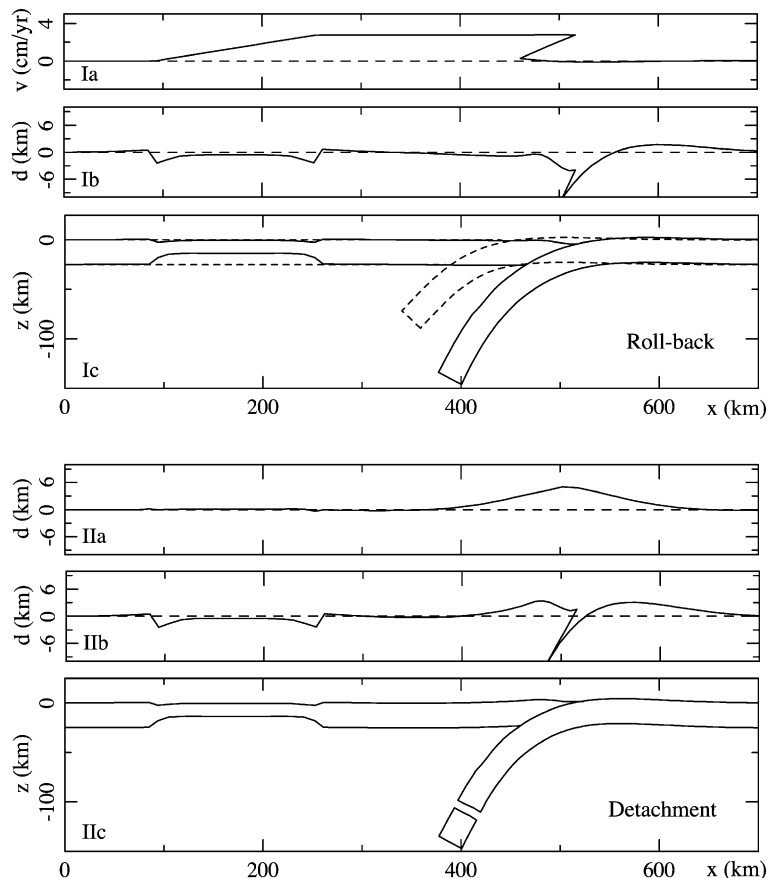


Fig. 4. Model RS0. As in Fig. 3 for subduction zone roll-back in a land-locked basin setting (e.g., Fig. 1a). The side boundaries of the surface plates are fixed laterally. The dip angle of the slab is free to change. (I) Roll-back results after 3.5 Ma (80 km of convergence across plate contact). (II) Detachment after 3.5 Ma.

around 3.5 km (Fig. 5I). The average rate of trench retreat is 3.1 cm/year.

3.1.2. Slab detachment

We use the three reference subduction models described above (S0, RS0 and RL0) to study the effects of detachment of subducted lithosphere on vertical surface displacements. Since we are interested primarily in those signals which result from the detachment, we simulate continued convergence until detachment, after which convergence stops. Detachment is imposed after 80 km of convergence, when model initialisation signatures have been overcome.

For the ongoing subduction setting, this is after 2 Ma (model S0 in Table 2). The average depth of the detachment fault is 106 km. Stresses due to viscous flow resulting from sinking of the detached part of lithosphere are not yet included (see Section 3.2). Detachment of the deeper part of the subducted lithosphere leads to a surface uplift which is 3–4 km at maximum (Fig. 3II). The topography on the overriding plate margin has a maximum height of around 1.5 km. This topography is the result of the phases of both subduction and detachment. The final net uplift is partly a consequence of the fact that we have included initial bending stresses. The uplift remains at the same value with time after detachment (Fig. 6)

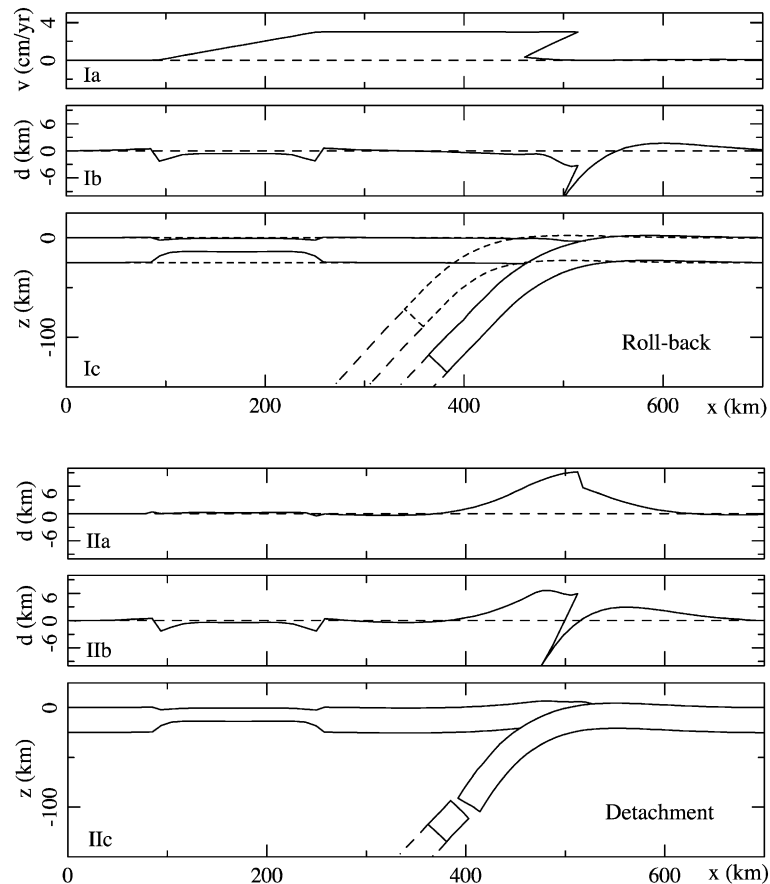


Fig. 5. Model RL0. As in Fig. 3 for subduction zone roll-back in a land-locked basin setting. The dip angle of the model slab end is fixed to simulate roll-back of a long slab. To indicate that the slab is considered long, the model slab end is shown extrapolated by long-dashed lines. (I) Roll-back results after 2.5 Ma (80 km of convergence across plate contact). (II) Detachment after 2.5 Ma.

Table 2
Model experiments

Model	Mode	Sd. depth ^a (km)	Sink parameter ^b	Uplift ^c (km)	Remark
S0	sub	106	–	3.2, 4.2	Figs. 3 and 7
S1	sub	106	–	4.5, 5.3	Subduction fault locked ^d
S2	sub	117	–	1.9, 2.3	Fig. 7
S3	sub	89	–	5.6, 8.2	Fig. 7
S4	sub	106	2, 50, 50	2.7, 3.3	Fig. 6
S5	sub	106	6, 50, 50	2.7, 3.4	Fig. 6
S6	sub	106	2, 100, 50	2.1, 2.6	Fig. 6
S7	sub	106	–	3.5, 4.9	F_{eff}^0 [–60, –100]
S8	sub	102	–	2.2, 3.2	$0.5 \times \Delta F^0$
RS0	roll	111	–	5.1, 4.0	Figs. 4 and 7
RS1	roll	124	–	2.9, 2.5	Fig. 7
RS2	roll	96	–	12.2, 8.8	Fig. 7
RL0	roll	103	–	8.9, 8.2	Fig. 5

^a Average depth of slab detachment.

^b v_{sink} (cm year^{–1}), $\Delta\rho$ (kg m^{–3}), a (km) (Eq. (1)).

^c Detachment after 80 km of convergence. Maximum uplift is measured right after detachment (left value) and 0.1 Ma later (right value).

^d After detachment.

since convergence has stopped and the elastic model is in equilibrium.

Maximum uplift for detachment in a closing basin setting is higher and amounts to approximately 5 km immediately after detachment for the case of a relatively short slab (model RS0, Fig. 4II). The surface topography has a maximum height of around 3.5 km. After the initial uplift, uplift decreases with time. This is caused by the low-viscosity zone in the overriding plate which takes up motion of the overriding plate away from the trench. The extensional back-arc basin, therefore, experiences a phase of compression after detachment.

Detachment of a long and wide slab in a closing basin setting results in a maximum uplift of approximately 9 km (model RL0, Fig. 5II). This value is higher than the uplift obtained for the case of roll-back of a short slab described above (model RS0). In comparison with the previous model, the imposed constraint on the deeper slab dip angle results in higher stresses in the subducting slab after the phase of retrograde motion, leading to higher uplift. During the phase of roll-back, the overriding plate margin subsided (Fig. 5I). Therefore, the resulting topography on this plate margin is around 6.7 km at maximum.

3.2. Parameter sensitivity

In the following, we examine (among others) how the surface displacements depend on depth of detachment, resistance to slip on the subduction fault after detachment, and viscous mantle flow due to sinking of the detached part.

In a limited time interval after detachment (on the order of several kyrs), motions on the subduction fault may be reverse to those which occur during subduction. As noted above, this induces a phase of compression in the back-arc basin for the roll-back models. The reversed motion is limited if friction on the subduction fault increases after detachment. This could be due to changes in fault stresses related to the uplift experienced by the lithospheric plates. An end-member case is obtained when the subduction fault completely locks after detachment. This leads to a higher surface uplift after slab detachment, for example, 4.5 km immediately after detachment for the case of non-migrating subduction (model S1 in Table 2, compare with 3.2 km for model S0).

In the reference models described above, detachment occurs at an average depth of around 100–110 km. The region of the future detachment fault is located just above the forcing interval — the depth interval in which F_{eff} is applied — at the start of

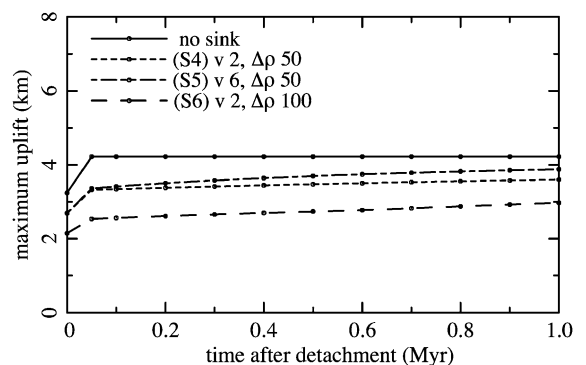


Fig. 6. Effect of viscous stresses due to sinking of the detached part of lithosphere on maximum uplift versus time after detachment. The surface uplift is initially reduced and recovers with time. The reference situation is the non-migrating subduction of model S0 (drawn line) with stresses due to sinking not included (see Fig. 3). Three dash/dotted lines are for different values for sinking velocity (v) and density difference ($\Delta\rho$) of the sphere in equation 1 of Appendix A (models S4, S5 and S6 in Table 2). The radius of the sphere is 50 km.

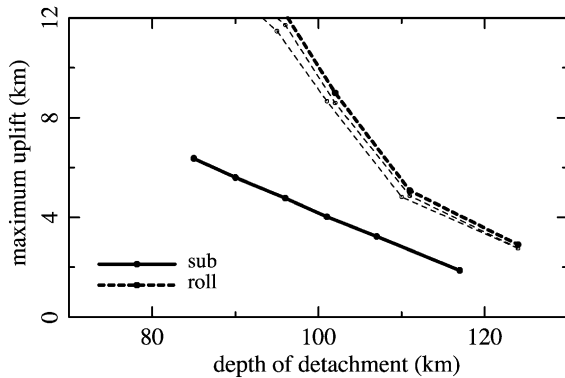


Fig. 7. Maximum uplift versus the depth of detachment. Drawn line: non-migrating subduction (model S0, Fig. 3). Dotted line: roll-back (model RS0, Fig. 4). For the roll-back model, the viscosity of the weak zone in the overriding plate is 10^{21} Pa s (bold curve), 10^{20} Pa s (upper light curve) and 5×10^{21} Pa s (lower light curve). Detachment is imposed after 80 km of convergence (2 Ma for model S0 and 3.5 Ma for model RS0.) Uplift is measured immediately after detachment. Small circles indicate obtained measurements.

subduction. Fig. 7 shows that the depth of detachment largely affects surface uplift (see also models S2, S3, RS1 and RS2 in Table 2). In case detachment is imposed at deeper levels, the magnitude of the in-plane tensional stresses in the region around the detachment fault is reduced. This reduces surface uplift. Detachment at shallower levels leads to larger surface uplifts. Once the future detachment fault has passed through the forcing interval, stresses in the slab around the fault hardly change during further subduction.

The uplift resulting from slab detachment is not very sensitive to the orientation of the detachment fault. In the ongoing subduction setting, detachment imposed on either a slab normal fault, a horizontal fault or a vertical fault results in a variation in uplift of not more than 0.5 km.

Sinking of the detached part of lithosphere in the viscous mantle will induce flow of mantle material. This flow generates dynamic pressure differences which lead to a downward displacement of the overlying surface. This deflection is reduced as the detached lithosphere sinks further down. To determine a first order of magnitude of this effect we use the equivalent of a sphere sinking in a viscous fluid below a free surface in the same manner as Chatelain et al. (1992) (see also Morgan, 1965) (Appendix A). The

sphere has a radius of 50 km and a density difference of 50 kg m^{-3} . Fig. 6 (model S4) shows that for the case of non-migrating subduction, the maximum surface uplift after detachment is reduced with 0.5–0.9 km compared with model S0 in which the viscous flow pressures are not included. In the period following detachment, uplift recovers by approximately 0.3 km during 1 Ma. During this time, the maximum uplift remains below the value for model S0. Uplift rate in the period after detachment is higher for a higher magnitude of the sinking velocity (model S5, Fig. 6). A larger density difference for the sphere further reduces the initial surface uplift (model S6). Using this simple analogue of a sinking sphere, we find that sinking of the detached part of lithosphere suppresses surface uplift due to detachment. The reduction is recovered in the period following detachment (see also Chatelain et al., 1992).

The calculated surface uplifts are affected by the choice of values for some of the parameters and boundary conditions in the subduction models, for example, effective pull force (F_{eff}) and the viscosity of the weak zone for the roll-back models. As discussed before, stresses in the subducting plate are the same for different values of v_{sub} as long as the same amount of convergence is considered. Model surface uplift is, therefore, not sensitive to the magnitude of convergence velocity. In all models discussed so far, F_{eff} is distributed over a depth interval of 60–80 km. The force interval is constrained to lie above the initial model slab end and below the region of large bending of the subducting plate. In case the force interval is extended to 60–100 km, surface uplift after detachment is somewhat higher (model S7). A change in buoyancy of the subducting material affects the dynamics of the subduction zone system leading to different surface topography (Buiter et al., 2001) and stresses in the subducting slab. For example, an increase in buoyancy — a decrease in ΔF in our model — decreases tensional stresses in the slab. This leads to lower uplift after detachment (model S8). For the roll-back models, the viscosity of the weak zone is one of the parameters which determine the velocity of trench retreat. In models with a high viscosity in the back-arc area, trench retreat is slow. The resistance to retreat could induce increased stresses in the subducting slab leading to higher uplift after detachment. Fig. 7 shows that the effect of viscosity of the weak zone

in the overriding plate is small for viscosities between 10^{20} and 5×10^{21} Pa s.

4. Discussion

4.1. Comparison with observations

No region exists in which slab detachment has unambiguously been identified. Furthermore, our model results can not straightforwardly be compared with observations for regions where detachment is suspected. Mountains at sites of continental collision indicate that high surface uplifts may accompany the final stages of a subduction zone system (e.g., the Alps, Carpathians, Himalayas). Such an uplift is the result of all processes active during collision, e.g., crustal thickening, thrusting and — possibly — slab detachment. Uplift due to detachment of subducted lithosphere, therefore, constitutes only part of the surface displacements which may be expected to occur during and after closure of an ocean.

We will here consider some examples of areas where surface uplift has been interpreted in the context of slab detachment. Timor in the Southern Banda Arc experienced an uplift of around 5 km from Mid-Pliocene to recent presumably related to detachment of the downgoing Australian plate (Audley-Charles, 1986; Price and Audley-Charles, 1987). Mitrovica et al. (1989) propose that Tertiary uplift in Western North America, with a maximum vertical displacement of at least 3 km, may be a consequence of either the termination of subduction or an increase in slab dip. The uplift is a tilt over a horizontal scale of hundreds of kilometres and, therefore, shows a spatial pattern quite different from our modelling results. Van der Meulen et al. (2000a) find an Early Pliocene uplift which is around 500 m for the Central Apennines foredeep (Italy) (see also Van der Meulen et al., 2000b). Their type of data is indicative of the minimum amount of uplift, so uplift could have been much higher. Calabria (Southern Italy) has experienced a surface uplift of approximately 700 m which may be due to detachment of the subducting Ionian lithosphere (Westaway, 1993). Chatelain et al. (1992) relate Quaternary uplifts of up to 500–700 m at the New Hebrides to slab detachment.

In comparison with these observations, the values we have calculated for uplift due to detachment are

rather high. Overlap exists with the reported values at the higher end of the observed range.

4.2. Continental collision and detachment

Detachment of subducted lithosphere is likely to occur in a situation in which a continental passive margin is being subducted (Davies and Von Blanckenburg, 1995; Wong et al., 1997). Our models do not intend to represent such a situation. Since we have not distinguished between oceanic and continental lithosphere (and their properties) in our models, the presented results may only be taken as first order indications of the surface displacements resulting from slab detachment after passive margin subduction.

4.3. Implications for the back-arc region

Retrograde motion of a subducting slab can only occur if the overriding plate allows it. The overriding plate must either be able to follow trench retreat or it extends. In our land-locked basin setting, we allow for roll-back through the introduction of a weak zone in the overriding plate. In this region, extension localises and a back-arc basin forms. Our modelling results indicate that in the period immediately following detachment, motion of the overriding plate may be reverse to motions occurring during the phase of roll-back. In that case, the back-arc basin experiences a phase of compression after detachment. This induces relative uplift of the basin surface which may lead to an erosional unconformity in the basin stratigraphy when back-arc subsidence subsequently continues. Further subsidence due to thermal relaxation may be expected for this overall extensional setting.

4.4. Uplift during subduction versus uplift following detachment

Our results indicate that the surface uplift induced by detachment of subducted lithosphere is a characteristic surface observable. To determine just how characteristic it is, we compare it to displacements which can occur during ongoing subduction. In a previous study (Buiter et al., 2001), we quantified vertical surface displacements resulting from changes in a subduction zone system, for example, variations in

buoyancy or friction along the interplate contact. We obtained a maximum surface uplift or subsidence on the order of 2–4 km. The displacements are mostly centred around the plate contact, on both the overriding and subducting plate margins. The surface uplift resulting from slab detachment is also centred around the plate contact. The range of magnitudes we have obtained encompasses the range of uplifts which can occur during ongoing subduction. Detachment at relatively shallow depths leads to uplifts which are much higher than can be expected during ongoing subduction. From our modelling results, we conclude that interpretation of the cause of uplift at a convergent plate margin requires that observations of the regional tectonic setting are taken into account.

4.5. Comparison with previous work

Our uplift is substantially higher than the uplift calculated by Schott and Schmeling (1998) or Mitrovica et al. (1989). One of the main differences between these dynamic models and our study is the lithospheric rheology which is viscous in the former models and elastic in ours. We expect that our modelling approach leads to an upper bound to surface uplift due to slab detachment (see also Section 4.6). In our model, stresses will remain at higher values with time. All deformation is elastic (except for the weak zone in the overriding plate) and is, therefore, recovered when forces are removed. This leads to a large uplift after detachment. Since the viscous models include the mantle in their computational domain, the effects of sinking of the detached part of lithosphere are taken into account in a consistent manner. Using the analogue of a sinking sphere (Chatelain et al., 1992), we find that sinking of the detached slab initially reduces surface uplift and that the reduction is recovered with time.

4.6. Model aspects

We have found that variations in calculated surface uplift after slab detachment are due to: (a) depth of detachment, (b) the effect of viscous stresses due to sinking of the detached part of lithosphere and their sensitivity to sinking velocity, (c) friction on the subduction fault after detachment and (d) the subduction model. Below, we discuss a number of con-

ceptual aspects of the modelling procedure which influence the uplift we have calculated.

(i) We impose very fast detachment. In reality, break-off will probably take some time. This does not affect surface uplift for our elastic rheology, but it can be important if a rheology with a viscous component were used. In that case, modelled surface uplifts may be reduced.

(ii) Since the model is two-dimensional, it is implied that detachment occurs at the same time and depth along the whole subduction zone. Three-dimensional aspects like lateral propagation of the detachment fault (Wortel and Spakman, 1992) are not included.

(iii) We use an effective elastic plate thickness to simulate the deflection behaviour of the lithosphere. Since our model is consistent in its definition of geometry, stresses and forces we believe that the calculated surface uplifts are a good first order approach to reality. The magnitude of the calculated uplifts is sensitive to the chosen value for the effective elastic thickness of the model plates. In this modelling study, we have shown results for one value of elastic plate thickness (25 km). To estimate the effect of a different elastic thickness we have varied the effective thickness with $\pm 20\%$ (5 km). For both non-migrating subduction and roll-back, the maximum uplift after detachment does not change with more than $\pm 10\%$.

(iv) In a continental collision setting, convergence will slow down until finally the subducted slab dangles in the mantle beneath the suture. Since viscous resistive stresses acting on the slab diminish with the reduction in subduction velocity, the slab experiences an increase in slab pull. This would induce a deepening of the Earth's surface. However, this deepening disappears after detachment when the whole pull force is removed — including the extra pull which was built up during the last phases of collision. Neglecting this additional pull force should, therefore, not affect net surface uplift if considered relative to the topography during subduction.

(v) The pull force F_{eff} is applied at a shallow depth interval. This results in tension in the slab which is constant for slab material which has passed through the force interval. An increase in resistance which the slab may experience at deeper depths, for example, due to the transition between upper and lower mantle, is not included in the model. It is, therefore, assumed

that the compression which may be induced by such a resistance is not transferred to the depths of detachment. In support, we note that the very occurrence of slab detachment indicates that the subducted slab must have been in tension.

5. Conclusions

Within the context of our elastic model, we find that detachment of subducted lithosphere may lead to a surface uplift of several kilometres near the plate margins. The uplift is sensitive to (a) the subduction phase preceding detachment, (b) depth of detachment, (c) friction along the subduction fault after detachment and (d) viscous stresses generated by sinking of the detached part of the slab. Our results are obtained for detachment at relatively shallow levels, i.e., around 100 km depth. For non-migrating subduction followed by detachment, we find maximum uplifts of 2–6 km, while for the case of roll-back this may be higher by 1–4 km. Since we use lithospheric plates with an effective elastic thickness, and study surface deformation immediately after rapid detachment, we expect that these values represent an upper bound to surface uplift due to slab detachment. Viscous flow due to sinking of the detached lithosphere initially reduces uplift (by several hundreds of metres at least). In case of subduction zone roll-back, the back-arc basin experiences a phase of compression following detachment.

The uplift values in part overlap vertical displacements which result from variations in an ongoing subduction situation (Buiter et al., 2001). Therefore, the regional tectonic setting should be taken into account when interpreting uplift observations in a convergent plate margin setting.

Acknowledgements

This work was conducted under the programme of the Vening Meinesz Research School of Geodynamics. During the investigations reported here, S. Buiter was financially supported by the Geosciences Foundation (GOA/ALW) of the Netherlands Organisation for Scientific Research (NWO). We thank Riad Hassani and an anonymous reviewer for their constructive reviews.

Appendix A. Stresses due to sinking of the detached slab

Sinking of the detached part of the slab causes flow of the viscous mantle. This flow generates pressure differences which lead to deflection of the overlying surface lithosphere. To take the effects of the sinking detached slab into account, we use the sinking of a sphere in a viscous medium below a free surface as a first order equivalent. This is a similar approach as that taken by Chatelain et al. (1992). The normal stress σ_n at the surface is (Morgan, 1965):

$$\sigma_n(r, D) = 2ga^3\Delta\rho \frac{D^3}{(r^2 + D^2)^{5/2}} \quad (1)$$

where r and D are horizontal distance and depth, respectively, to the centre of the sphere, a is the radius of the sphere and $\Delta\rho$ is the density difference between the sphere and its surrounding medium. This expression is valid for $a < D$ and is accurate to second order in a/D . It is assumed that the viscosity of the mantle does not vary with depth. The mantle viscosity does not appear in Eq. (1) due to the following reason: The normal stress depends (among others) on viscosity and the sinking velocity. The sinking velocity depends inversely on viscosity, its substitution into the expression for the normal stress, therefore, cancels the viscosity variable.

A sphere relatively near to the surface leads to a high value for the normal stress. This stress causes a downward surface deflection. As the sphere sinks further down the depth D increases, the normal stress decreases and the downward deflection is reduced. A heavy (high $\Delta\rho$), large (high a) sphere will generate a larger normal stress than a light, small sphere.

We apply the normal stresses of the sinking sphere equivalent to lithosphere nearest to the sinking detached lithosphere. Every calculation step the stresses of Eq. (1) are evaluated and compared with the value of the stresses in the previous calculation step. This stress difference is then applied.

References

- Audley-Charles, M.G., 1986. Rates of Neogene and Quaternary tectonic movements in the Southern Banda Arc based on micro-palaeontology. *J. Geol. Soc. (Lond.)* 143, 161–175.

- Buiter, S.J.H., Govers, R., Wortel, M.J.R., 2001. A modelling study of vertical surface displacements at convergent plate margins. *Geophys. J. Int.* 147, 415–427.
- Caldwell, J.G., Haxby, W.F., Karig, D.E., Turcotte, D.L., 1976. On the applicability of a universal elastic trench profile. *Earth Planet. Sci. Lett.* 21, 239–246.
- Carminati, E., Giunchi, C., Argnani, A., Sabadini, R., Fernandez, M., 1999. Plio-Quaternary vertical motion of the Northern Apennines: insights from dynamic modelling. *Tectonics* 18, 703–718.
- Chatelain, J., Molnar, P., Prévot, R., Isacks, B., 1992. Detachment of part of the downgoing slab and uplift of the New Hebrides (Vanuatu) islands. *Geophys. Res. Lett.* 19, 1507–1510.
- Christensen, U.R., 1996. The influence of trench migration on slab penetration into the lower mantle. *Earth Planet. Sci. Lett.* 140, 27–39.
- Davies, G.F., 1995. Penetration of plates and plumes through the mantle transition zone. *Earth Planet. Sci. Lett.* 133, 507–516.
- Davies, H.J., Von Blanckenburg, F., 1995. Slab breakoff: a model of lithospheric detachment and its test in the magmatism and deformation of collisional orogens. *Earth Planet. Sci. Lett.* 129, 85–102.
- DeMets, C., Gordon, R.G., Argus, D.F., Stein, S., 1994. Effect of recent revisions to the geomagnetic reversal time scale on estimates of current plate motions. *Geophys. Res. Lett.* 21, 2191–2194.
- Dvorkin, J., Nur, A., Mavko, G., Ben-Avraham, Z., 1993. Narrow subducting slabs and the origin of backarc basins. *Tectonophysics* 227, 63–79.
- Fuchs, K., Bonjer, K.-P., Bock, G., Comea, I., Radu, C., Enescu, D., Jianu, D., Nourescu, A., Merkle, G., Moldoveanu, T., Tudorache, G., 1979. The Romanian earthquake of March 4, 1977: II. Aftershocks and migration of seismic activity. *Tectonophysics* 53, 225–247.
- Garfunkel, Z., Anderson, C.A., Schubert, G., 1986. Mantle circulation and the lateral migration of subducted slabs. *J. Geophys. Res.* 91, 7205–7223.
- Giunchi, C., Sabadini, R., Boschi, E., Gasperini, P., 1996. Dynamic models of subduction: geophysical and geological evidence in the Tyrrhenian Sea. *Geophys. J. Int.* 126, 555–578.
- Gurnis, M., Eloy, C., Zhong, S., 1996. Free-surface formulation of mantle convection—II. Implication for subduction-zone observables. *Geophys. J. Int.* 127, 719–727.
- Hassani, R., Jongmans, D., Chéry, J., 1997. Study of plate deformation and stress in subduction processes using two-dimensional models. *J. Geophys. Res.* 102, 17951–17965.
- Hippolyte, J.-C., Angelier, J., Roue, F., 1994. A major geodynamic change revealed by Quaternary stress patterns in the Southern Apennines (Italy). *Tectonophysics* 230, 199–210.
- Isacks, B., Molnar, P., 1969. Mantle earthquake mechanisms and the sinking of the lithosphere. *Nature* 223, 1121–1124.
- McKenzie, D.P., 1969. Speculations on the consequences and causes of plate motions. *Geophys. J. R. Astron. Soc.* 18, 1–32.
- Meijer, P.Th., Wortel, M.J.R., 1996. Temporal variations in the stress field of the Aegean region. *Geophys. Res. Lett.* 23, 439–442.
- Melosh, H.J., Raefsky, A., 1980. The dynamical origin of subduction topography. *Geophys. J. R. Astron. Soc.* 60, 333–354.
- Melosh, H.J., Raefsky, A., 1983. Anelastic response of the earth to dip slip earthquakes. *J. Geophys. Res.* 88, 515–526.
- Melosh, H.J., Williams Jr., C.A., 1989. Mechanics of graben formation in crustal rocks: a finite element analysis. *J. Geophys. Res.* 94, 13961–13973.
- Mitrovica, J.X., Beaumont, C., Jarvis, G.T., 1989. Tilting of continental interiors by the dynamical effects of subduction. *Tectonics* 8, 1079–1094.
- Morgan, W.J., 1965. Gravity anomalies and convection currents. *J. Geophys. Res.* 70, 6175–6187.
- Oncescu, M.C., Burlacu, V., Anghel, M., Smalbergher, V., 1984. Three-dimensional P-wave velocity image under the Carpathian arc. *Tectonophysics* 106, 305–319.
- Pascal, G., Dubois, J., Barazangi, M., Isacks, B.L., Oliver, J., 1973. Seismic velocity anomalies beneath the New Hebrides island arc: evidence for a detached slab in the upper mantle. *J. Geophys. Res.* 78, 6998–7004.
- Price, N.J., Audley-Charles, M.G., 1987. Tectonic collision processes after plate rupture. *Tectonophysics* 140, 121–129.
- Ritsema, A.R., 1972. Deep earthquakes of the Tyrrhenian Sea. *Geol. Mijnb.* 51, 541–545.
- Schott, B., Schmeling, H., 1998. Delamination and detachment of a lithospheric root. *Tectonophysics* 296, 225–247.
- Sorel, D., Mercier, J., Keraudren, B., Cushing, M., 1988. The role of slab-pull force in the Plio-Pleistocene geodynamic evolution of the Aegean arc: subsidence and uplift of the external arc and changes in the tectonic regime. *C. R. Acad. Sci., Paris t* 307, 1981–1986.
- Spakman, W., 1990. Tomographic images of the upper mantle below central Europe and the Mediterranean. *Terra Nova* 2, 542–553.
- Spakman, W., Wortel, M.J.R., Vlaar, N.J., 1988. The Hellenic subduction zone: a tomographic image and its geodynamic implications. *Geophys. Res. Lett.* 15, 60–63.
- Turcotte, D.L., Schubert, G., 1982. *Geodynamics: Applications of Continuum Physics to Geological Problems*. Wiley, New York, 450 pp.
- Van der Meulen, M.J., Buiter, S.J.H., Meulenkaamp, J.E., Wortel, M.J.R., 2000a. An early Pliocene uplift of the central Apenninic foredeep and its geodynamic significance. *Tectonics* 19, 300–313.
- Van der Meulen, M.J., Kouwenhoven, T.J., Van der Zwaan, G.J., Meulenkaamp, J.E., Wortel, M.J.R., 2000b. Late Miocene uplift in the Romagnan Apennines and the detachment of subducted lithosphere. *Tectonophysics* 315, 315–331.
- Van der Voo, R., Spakman, W., Bijwaard, H., 1999. Mesozoic subducted slabs under Siberia. *Nature* 397, 246–249.
- Van de Zedde, D.M.A., Wortel, M.J.R., 2001. Shallow slab detachment as a transient source of heat at mid-lithospheric depths. *Tectonics* 20, 868–882.
- Von Blanckenburg, F., Davies, J.H., 1995. Slab breakoff: a model for syncollisional magmatism and tectonics in the Alps. *Tectonics* 14, 120–131.
- Wallace, M.H., Melosh, H.J., 1994. Buckling of a pervasively faulted lithosphere. *Pure Appl. Geophys.* 142, 239–261.
- Watts, A.B., Talwani, M., 1974. Gravity anomalies seaward of deep-sea trenches and their tectonic implications. *Geophys. J. R. Astron. Soc.* 36, 57–90.

- Westaway, R., 1993. Quaternary uplift of Southern Italy. *J. Geophys. Res.* 98, 21741–21772.
- Wong, A., Ton, S.Y.M., Wortel, W., 1997. Slab detachment in continental collision zones: an analysis of controlling parameters. *Geophys. Res. Lett.* 24, 2095–2098.
- Wortel, M.J.R., Spakman, W., 1992. Structure and dynamics of subducted lithosphere in the Mediterranean region. *Proc. Kon. Ned. Akad. Wetensch.* 95, 325–347.
- Wortel, M.J.R., Spakman, W., 2000. Subduction and slab detachment in the Mediterranean–Carpathian region. *Science* 290, 1910–1917.